buildings

MDPI

Article

Experimental Research on Axial Compression Performance of High-Performance-Fiber-Reinforced-Cement-Composite-Prefabricated Monolithic Composite Columns

Tingting Lu, Haowei Jin * and Kai Guan

School of Civil Engineering, Xijing University, Xi'an 710123, China; lutingbstu@126.com (T.L.); xjdxgkai@163.com (K.G.)
* Correspondence: jhw523@163.com

Abstract: In order to improve the mechanical properties of prefabricated monolithic composite columns, high-performance fiber-reinforced cement composite (HPFRCC) material was used to prefabricate mold shells and form a composite column with post-cast ordinary concrete. Axial compression tests were conducted on five HPFRCC-prefabricated shell composite columns and one RC prefabricated shell composite column to study the mechanical performances of prefabricated monolithic composite columns. The influences of the volume stirrup ratio, the longitudinal reinforcement ratio, and the shell material on axial compression performance were also studied. The results showed that using HPFRCC-prefabricated shells could improve the deformation performance of the composite column. The compressive strain corresponding to the yielding load of the HPFRCC-prefabricated formwork column was 23.85% higher than that of the RC-prefabricated shell composite column, and the compressive strain corresponding to the peak load increased by 26.72%. The longitudinal reinforcement ratio slightly affected the axial compression bearing capacity of the prefabricated shell composite column. Compared with ECCT−01, the peak load of ECCT−04 increased by 0.6%, and the peak load of ECCT−05 increased by 1.4%. As the volume stirrup ratio increased, the deformation performance of the HPFRCC-prefabricated composite column improved. Compared with ECCT−01, the compressive strain corresponding to the yield load and peak load of ECCT−02 increased by 24.21% and 7.33%, respectively. The compressive strain values corresponding to the yield load and peak load of ECCT−03 decreased by 25.58% and 24.01%, respectively.

Keywords: composite column; HPFRCC material; axial compression performance; prefabricated shell

check for updates

Citation: Lu, T.; Jin, H.; Guan, K. Experimental Research on Axial Compression Performance of High-Performance-Fiber-Reinforced-Cement-Composite-Prefabricated Monolithic Composite Columns. *Buildings* **2023**, *13*, 1748. https://doi.org/10.3390/buildings13071748

Academic Editor: Hossam El-Din Mohammad Sallam

Received: 8 June 2023
Revised: 29 June 2023
Accepted: 4 July 2023
Published: 10 July 2023

Copyright: © 2023 by the authors. Licensee MDPI, Basel, Switzerland. This article is an open access article distributed under the terms and conditions of the Creative Commons Attribution (CC BY) license (https://creativecommons.org/licenses/by/4.0/).

1. Introduction

Compared with traditional concrete, high-performance fiber-reinforced cement composite (HPFRCC) material exhibits good tensile properties with microcrack and strain hardening characteristics. Due to the high cost of pure HPFRCC components, the applications of HPFRCC material are limited. Thus, the concept and technology of composite columns have been proposed. Some scholars [1,2] studied the axial compression performance of steel tube–concrete (containing steel fiber) columns and showed that the compression performance of the composite column was significantly improved, and the incorporation of steel fibers did not change the failure mode of the specimen. Wang et al. [3] studied composite columns equipped with steel fiber RPC permanent column molds under a static load and showed that the steel fiber RPC column formworks had a specific tight band restraint effect on the core columns. In recent years, more and more scholars [4–9] have begun to study concrete with PVA fibers, and its strain-hardening characteristics and micro-crack characteristics can effectively improve the energy dissipation capacity and deformation capacity of concrete components. Daugevicius et al. [10] studied the performance of concrete and reinforced concrete elements reinforced with high-performance fiber-reinforced cement concrete (HPFRCC) shells. The results showed that HPFRCC materials could obtain the

best reinforcement effect on ordinary concrete elements and changed the failure mode of concrete elements from brittle failure to ductile failure. Liang et al. [11] studied the seismic performance of prefabricated formwork columns, and their results showed that under the same conditions, the seismic performance of the specimen with a UHPC formwork plus a 10 mm concrete protective layer was relatively good. Cheng et al. [12] studied the axial compression of reinforced concrete columns reinforced with a fiber-braided mesh, and their results showed that the failure form and deformation of the columns were both effectively improved. Cai et al. [13] conducted axial compression tests on concrete-filled steel tubular columns wrapped in engineered cement composite materials, and their results showed that the composite columns exhibited a higher load-bearing capacity and improved ductility. Li et al. [14] used a polypropylene composite material as the prefabricated formwork to pour a composite column made of ordinary concrete and studied axial compression on ordinary integral concrete columns and pure ECC concrete columns. The results showed that the bearing capacity, ductility, and peak strength were all significantly improved. Wang et al. [15] used a high-strength steel strand mesh combined with ECC to strengthen a reinforced concrete column for eccentric compression research, and their results showed that the bearing capacity and ductility of the composite column were significantly improved. Charles et al. [16] showed that the differential quadrature method (DQM) was indeed a powerful technique for the analysis of composite plates. Wang et al. [17] presented a new framework for stress analysis of three-dimensional (3D) composite (multi−layered) elastic materials by using a meshless generalized finite difference method (GFDM), which showed great promise in the analysis of 3D elastic composite materials. Kefal et al. [18] used the inverse finite element method (iFEM) algorithm combined with the kinematic relations of refined zigzag theory (RZT), which showed very good consistency when compared to the results of DIC/FEM analysis and experimental strains. Kabir et al. [19] presented a computationally efficient technique based on Bézier curves that predicted the composite elastic constants more accurately than other common methods.

In order to improve the mechanical performance of the prefabricated monolithic composite column, the HPFRCC material was used to prefabricate molded shells. The effects of factors, such as the volume stirrup ratio, the longitudinal reinforcement ratio, and the shell material, on the axial compression performance of the HPFRCC-prefabricated monolithic composite column were studied.

2. Experimental Design

2.1. Specimen Design

Axial compression tests were carried out on six columns. The specimens were numbered ECCT−01, ECCT−02, ECCT−03, ECCT−04, ECCT−05, and RCT−01. The six column specimens were composed of prefabricated shells and post-cast internal concrete. The prefabricated shells of ECCT−01~05 were made of HPFRCC material, and the interiors of ECCT−01~05 were post-cast ordinary concrete. The prefabricated shell and the internal post-cast concrete of RCT−01 were ordinary concrete. The designed shear–span ratio of the specimen was 3, the cross-sectional dimensions of the column were 250 × 250 mm, the height was 750 mm, and the thickness of the prefabricated shell was 30 mm. Three cube blocks of 100 × 100 × 100 mm, three prismatic compression blocks of 100 × 100 × 300 mm, and three dumbbell-shaped blocks were cast and cured at the same time with the column. Details of the size of the test pieces can be found in Figure 1, and detailed parameters of the column specimens are shown in Table 1.

2.2. Material Properties

The grade of the ordinary concrete used for the specimens was C40. HPFRCC material was mixed from Conch P.O. 42.5 Portland cement, first-grade fly ash, quartz sand, and PVA fiber. The volume admixture of PVA fiber was 2%. The performance parameter of the PVA fiber is shown in Table 2. The grade of the longitudinal bars was HRB400 and the grade of the stirrups was HPB300. The cubic compressive strength (f_{cu}) and the

prismatic compressive strength (f_c) of ordinary concrete and HPFRCC materials were measured through compressive tests on the corresponding blocks. The tensile strength (f_t) of HPFRCC materials was measured through tension tests on the dumbbell-shaped blocks. The pouring process of the test specimens is shown in Figure 2. The properties of the material are shown in Table 3 and the tensile stress–strain curve is shown in Figure 3.

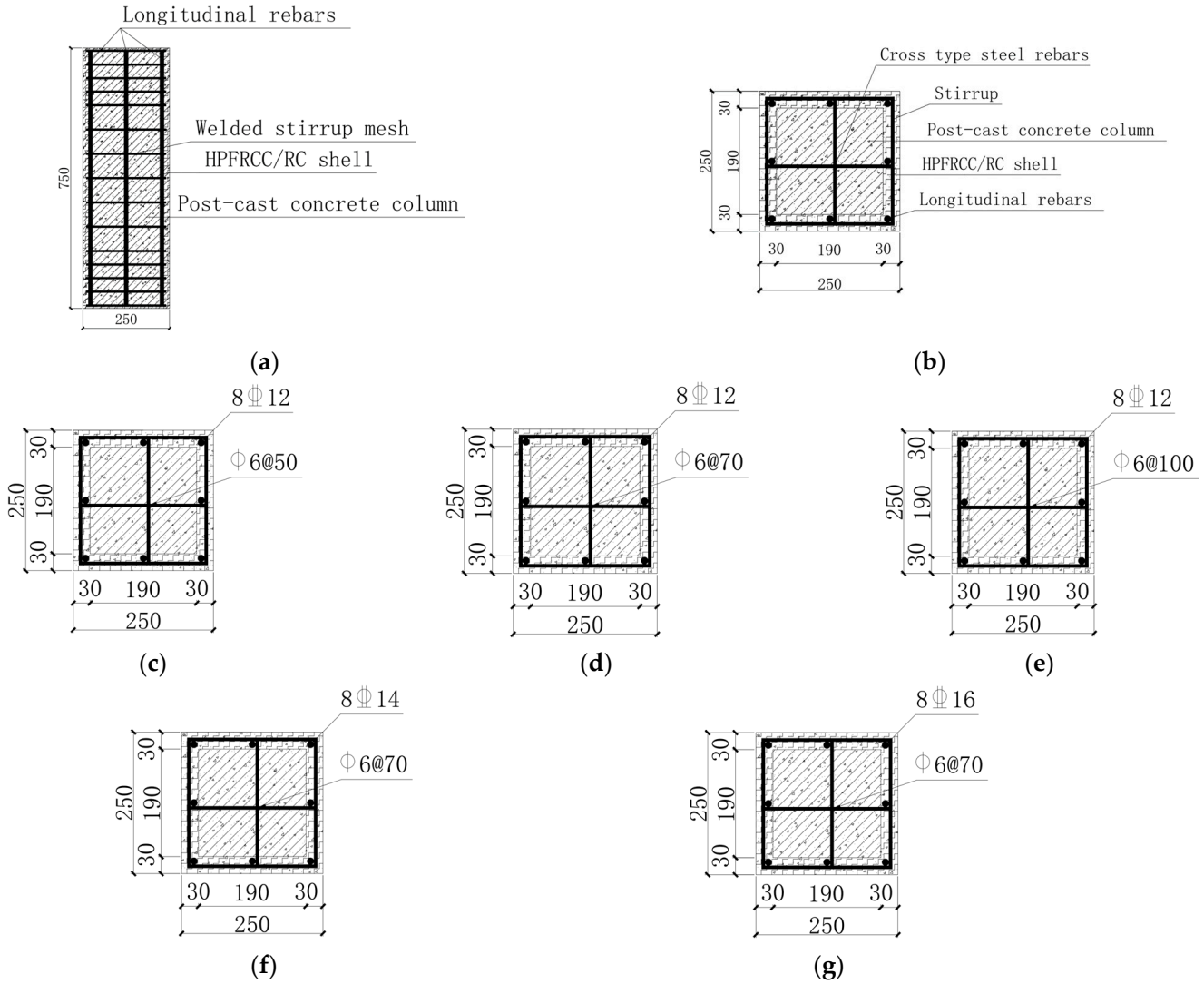


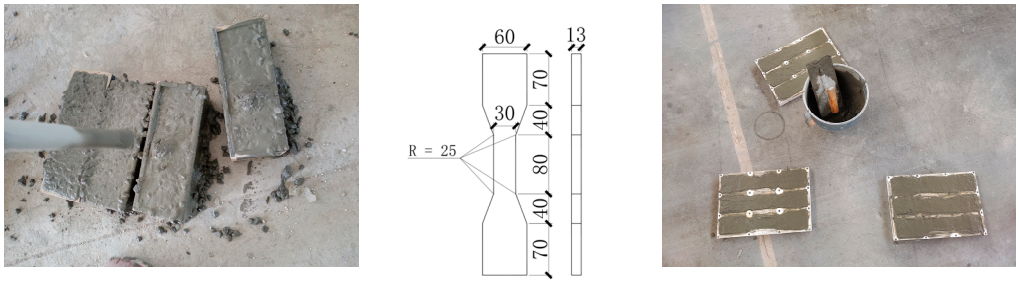
Figure 1. Specimen size details. (**a**) Sectional diagram. (**b**) Cross-sectional diagram. (**c**) Rebar reinforcement diagram of ECCT−02. (**d**) Rebar reinforcement diagram of ECCT−01 and RCT−01. (**e**) Rebar reinforcement diagram of ECCT−03. (**f**) Rebar reinforcement diagram of ECCT−04. (**g**) Rebar reinforcement diagram of ECCT−05.

Table 1. Parameters of the columns.

Test Piece Number	Longitudinal Rebar Ratio/%	Volume Ratio ρ_v/%	Longitudinal Tendons	Stirrup
ECCT−01	1.45	1.05	8C12	A6@70
ECCT−02	1.45	1.48	8C12	A6@50
ECCT−03	1.45	0.74	8C12	A6@100
ECCT−04	1.97	1.05	8C14	A6@70
ECCT−05	2.57	1.05	8C16	A6@70
RCT−01	1.45	1.05	8C12	A6@70

Table 2. PVA fiber performance parameters.

Density/ ($g \cdot cm^{-3}$)	Tensile Strength/ MPa	Elastic Modulus/ GPa	Length/ mm	Elongation Rate/ %
1.3	1600	42	12	7



(**a**) (**b**) (**c**)

Figure 2. Test block pouring process. (**a**) Poured prismatic test blocks. (**b**) Tensile test piece size chart. (**c**) Poured tensile test pieces.

Table 3. Concrete/HPFRCC mechanical properties parameters.

Material Name	f_{cu}/MPa	f_c/MPa	f_t/MPa
HPFRCC	50.9	40.2	5.6
Regular concrete	49.3	38.2	3.3

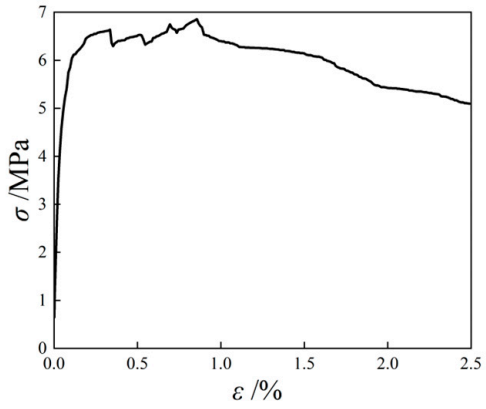


Figure 3. The tensile stress–strain curve of HPFRCC material.

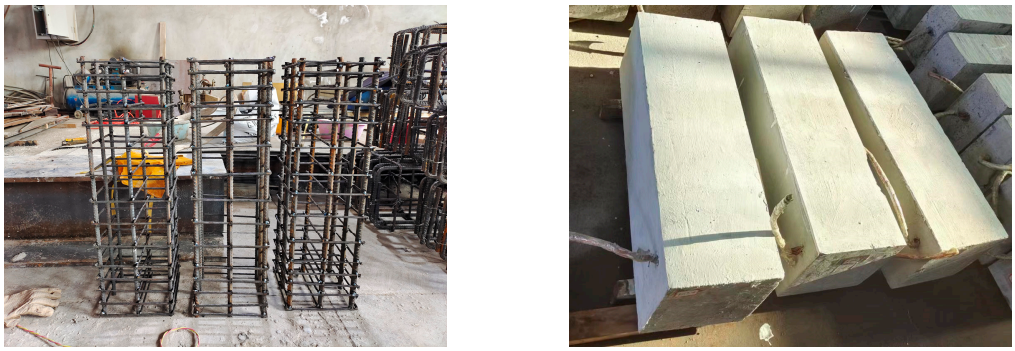
2.3. Specimen Fabrication

The HPFRCC/RC-prefabricated shell composite column was casted side by side. The rebar-welded meshes were made first. The stirrups and longitudinal bars were connected by welding. Then, the mold shell was prefabricated, and finally, the core concrete was poured. The actual specimen is shown in Figure 4.

2.4. Test Loading and Measurement

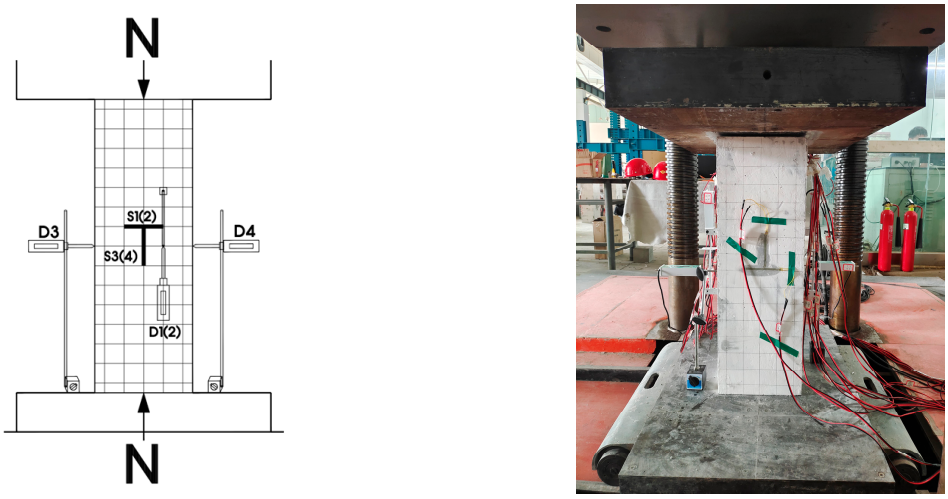
The axial compression test was conducted through the 5000 kN electro−hydraulic servo pressure tester. The test setup and instruments are shown in Figure 5. The specimen was placed in the correct position, and a level for vertical calibration was used to prevent local compression damage. Before the formal test, the composite column specimen was preloaded to eliminate the contact gap between the composite columns and the pressure plate of the testing machine. The loading process was displacement-controlled for safety. The tests were loaded at a constant speed. The loading speed was 0.2 mm/min, every

displacement of each level was 0.3 mm, and the load was then sustained for 120 s. The purpose of sustaining the load was to give the structure time to deform fully under load, as well as time for observation and analysis of the experiments conducted during that time. The data acquisition frequency of the WDW electronic universal testing machine control system was 10 Hz. Grids (50 mm × 50 mm) were drawn on the surface of the composite column before the test to observe the development of the crack more intuitively. When the cracks appeared or extended, they would be drawn with a pencil to record their development. When the crack width increased, the crack width measuring instrument was used to monitor the crack width. The test was stopped when the load dropped to 60% of the peak load.



(**a**) (**b**)

Figure 4. Diagram of column specimen fabrication. (**a**) Steel skeleton. (**b**) Forming diagram of HPFRCC column.



(**a**) (**b**)

Figure 5. Schematic diagram of the test. (**a**) Test loading details. (**b**) Test loading device.

The strains of rebar and concrete were measured through resistance strain gauges, and the strain gauges were arranged as shown in Figure 6. Two displacement sensors (D1, D2) were symmetrically arranged to monitor the axial deformation of the specimen. Two horizontal displacement sensors (D3, D4) were symmetrically arranged to measure the transverse deformation of the column. Two transverse strain gauges (S1, S2) and two longitudinal strain gauges (S3, S4) were symmetrically arranged on the concrete to monitor the stain of the concrete. The data were recorded by the DHDAS dynamic signal acquisition and analysis system. The instrument layout is shown in Figures 5 and 7.

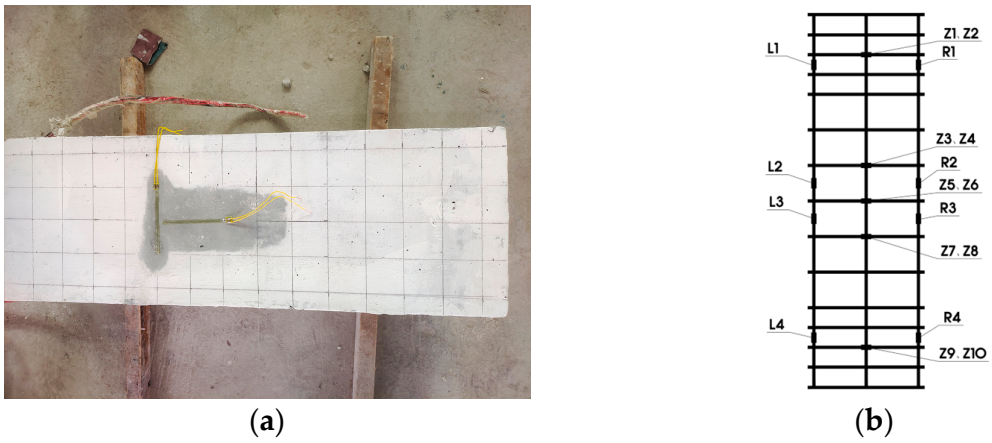


Figure 6. Strain gauge pasting layout. (**a**) Concrete strain gauge location. (**b**) Rebar strain gauge location.

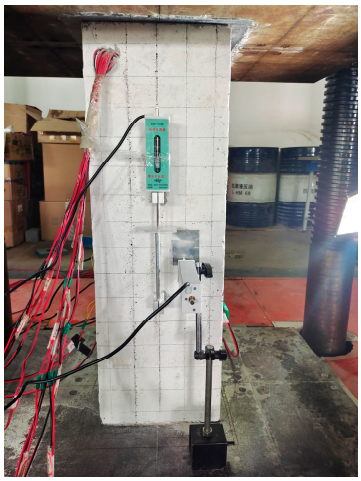


Figure 7. Displacement meter layout.

3. Experimental Results and Discussion

3.1. Crack Development and Failure Form

Figure 8 shows a diagram of the failure form of the specimen columns.

(1) For the specimen RCT−01 column, there was no obvious phenomenon at the initial loading stage. As the load increased, when the load reached 450 kN, vertical cracks appeared at the top of the RCT−01 column. As the load increased, the cracks continued to extend. When the load reached 1100 kN, the vertical crack length extended to 10 cm. When the load reached 2550 kN, vertical cracks appeared for the first time in the lower part of the specimen. At the same time, the vertical cracks extended from top to bottom and eventually formed a penetrating crack. When the load reached the peak load, the RC-prefabricated shell underwent dense cracking, accompanied by continuous spalling of small pieces of the shell. After reaching the peak load, the specimen was suddenly destroyed, and the load dropped to 1934 kN. The test was stopped. The vertical cracks at the top and bottom of the column expanded, the outer casing at the corners collapsed and fell, and the fragments fell at the intersection of the cracks; the concrete at the corners was crushed, a large area of concrete spalled, and the internal steel bars were exposed.

(2) For the ECCT−01 specimen, when the load reached 1000 kN, several minor vertical cracks appeared at the top of the column and the length was 40 mm. As the load increased, the crack continued to develop. When the load reached 2470 kN, the crack penetrated vertically. When the load reached 2640 kN, the transverse crack in the

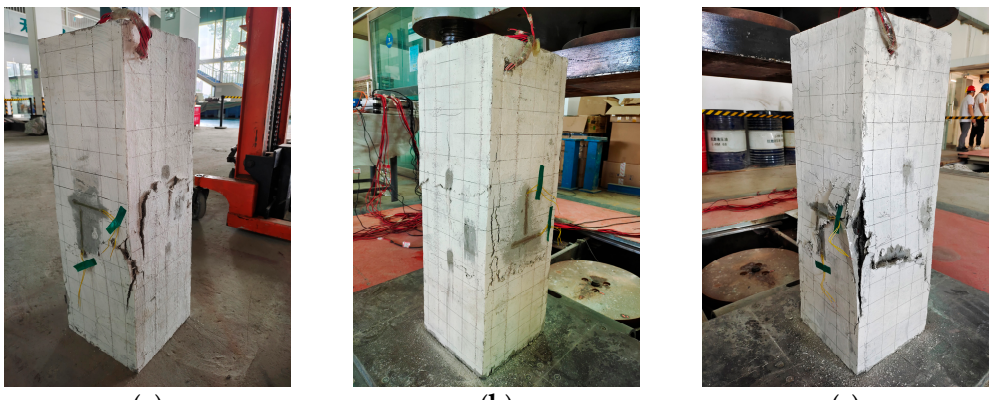
middle of the specimen was connected. When the load reached the peak load, the concrete in the middle of the specimen cracked outward transversely. Then, the load showed a downward trend. When the load decreased to 2095 kN, the vertical cracks at the top and bottom of the column expanded with a width of about 3 mm, and the HPFRCC shell cracked at the corners of the lower and middle parts of the column.

(3) For the ECCT−02 specimen, when the load reached 680 kN, a minor vertical crack appeared at the top of the column, located at the top right of the specimen, with a length of 43 mm. As the load increased, the crack continued to develop. When the load reached 940 kN, a transverse crack appeared at a position 17 cm from the top of the column, with a length of 10 cm. When the load reached the peak load, a thorough S-shaped transverse crack appeared in the middle of the specimen. When the load dropped to 1832 kN, the test was stopped. The right corner of the middle and upper part of the column cracked, a 30 cm-long shell sheet fell, and the width of the vertical crack near the cracked corner increased to 5 mm.

(4) For the ECCT−03 specimen, three transverse cracks with different positions appeared in the middle of the specimen when the load reached 1030 kN, with lengths of 5 cm, 8 cm, and 10 cm. When the load reached the peak load, several minor vertical cracks appeared from the top of the specimen, and the transverse crack in the middle penetrated. Then, the load showed a downward trend. When the load dropped to 1765 kN, the maximum width of the crack was 5 mm.

(5) When the load reached 810 kN, micro-cracks in the middle of the ECCT−04 specimen began to appear. As the load increased, cracks continued to develop in the middle of the specimen. When the load reached 1410 kN, there were multiple minor transverse cracks, the upper and lower interval was 5 cm and the length was 15 cm. When the load reached the peak load, a transverse convex crack developed outward in the concrete in the middle of the specimen. When the load dropped to 1960 kN, the vertical cracks at the lateral edge of the middle of the column expanded with a width of 4 mm, and dense cracks appeared in the HPFRCC shell at the corners.

(6) There was no phenomenon on the surface of the ECCT−05 specimen at the initial loading stage. When the load reached 1000 kN, vertical cracks started appearing in the column's upper part, 3 cm from the top and 4 cm long. When the load reached 1700 kN, a transverse crack appeared in the middle of the specimen with a length of 3 cm, the vertical crack extended from the top to the middle, and the length was 20 cm. When the load reached the peak load, the vertical crack in the middle of the specimen ran obliquely from top to bottom. Continuing with the displacement loading, the load showed a downward trend. When the load dropped to 2032 kN, the longitudinal crack at the bottom of the column expanded, and the widest part of the crack was 15 mm. The middle part of the column produced a minor transverse crack, which was slightly convex. The outer shell at the corners showed a chipped appearance.



(**a**) (**b**) (**c**)

Figure 8. *Cont.*



(**d**) (**e**) (**f**)

Figure 8. Failure patterns of HPFRCC/RCT specimens. (**a**) ECCT−01. (**b**) ECCT−02. (**c**) ECCT−03. (**d**) ECCT−04. (**e**) ECCT−05. (**f**) RCT−01.

As mentioned above, compared with the RC-prefabricated shell monolithic composite column, the HPFRCC-prefabricated shell improved the deformation performance of the composite column, and the composite column maintained better integrity. The increase in the volume hoop ratio enhanced the restraint effect of the formwork and improved the deformation capacity of the composite column.

3.2. Axial Load—Axial Deformation Curve and Parameter Analysis

The main characteristic point parameters of the six specimens are shown in Tables 4 and 5, and the axial load−axial displacement curves of the six specimens are shown in Figure 9.

Table 4. Column specimen load and compressive strain.

Test Piece Number	Yield Load/kN	Yield Pressure Strain/10^{-6}	Peak Load/kN	Peak Pressure Strain/10^{-6}
ECCT−01	2625.35	7771.18	3179.82	9511.28
ECCT−02	2904.47	9652.34	3133.84	10,208.67
ECCT−03	2568.13	6188.56	3074.38	7224.52
ECCT−04	2670.92	8220.32	3197.91	12062.67
ECCT−05	2738.34	7180.47	3227.32	8465.33
RCT−01	2561.32	5918.68	3204.43	6970.67

Table 5. Feature point secant stiffness.

Test Piece Number	Peak Load/kN	Peak Point Secant Stiffness (Mpa/mm)	Failure Load/kN	Yield Point Secant Stiffness/(Mpa/mm)
ECCT−01	3179.83	−1.52	2543.81	26.43
ECCT−02	3133.82	−2.36	2507.03	16.48
ECCT−03	3074.24	0.53	2459.44	15.66
ECCT−04	3197.93	−44.15	2558.31	43.58
ECCT−05	3228.31	−2.50	2582.62	8.68
RCT−01	3204.42	−4.24	2563.53	41.70

3.2.1. Effect of Prefabricated Shell Material

As listed in Table 5, compared with RCT−01, the yield load of ECCT−01 increased by 10.63%, the compressive strain corresponding to the yield load increased by 23.85%, and the compressive strain corresponding to the peak load increased by 26.72%. It can be seen that the HPFRCC-prefabricated shell had a significant impact on the deformation ability of the column specimen. The use of HPFRCC material in the prefabricated formwork can effectively improve the deformation capacity of the composite column. HPFRCC material exhibits microcracks and pseudo-strain-hardening characteristics and has a good tensile

deformation ability. These properties made the HPFRCC material continue to be stressed with the steel bar after cracking. Therefore, the shell prefabricated with HPFRCC material can provide additional restraint to the core concrete. At the same time, the yielding of longitudinal reinforcement was also delayed. Then, the deformation ability of the composite column was improved by using the HPFRCC material.

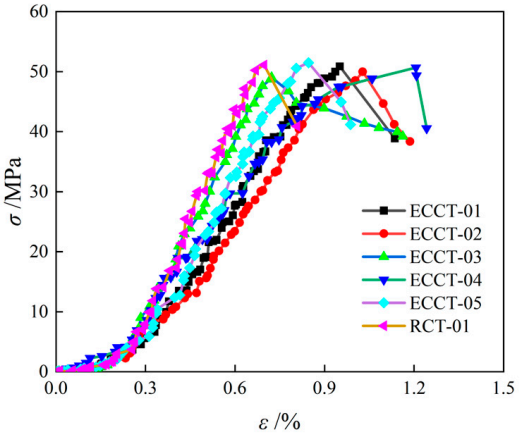


Figure 9. Axial stress−strain curve.

3.2.2. Effect of Longitudinal Bar Reinforcement Ratio

In Table 5, compared with ECCT−01, the yield load of ECCT−04 increased by 1.7% and the yield load of ECCT−05 increased by 4.3%. The peak load of ECCT−04 increased by 0.6% and the peak load of ECCT−05 increased by 1.4%. As the longitudinal reinforcement ratio increased, the peak load increased in the axial compression test. The increase in the longitudinal reinforcement ratio can make the composite column have a relatively high bearing capacity.

3.2.3. Effect of Volume Stirrup Ratio

Compared with ECCT−01, the yield load of ECCT−02 increased by 10.63% and the yield load of ECCT−03 decreased by 2.26%; the compressive strain corresponding to the yield load of ECCT−02 increased by 24.21%; the compressive strain corresponding to the yield load of ECCT−03 decreased by 25.58%; the compressive strain corresponding to the peak load of ECCT−02 increased by 7.33%; and the compressive strain corresponding to the peak load of ECCT−03 decreased by 24.01%. It can be seen that the volume stirrup ratio has a certain influence on the yield load and the corresponding compressive strain of HPFRCC specimens. The larger the volume stirrup ratio of HPFRCC columns, the greater the deformation performance. The stirrups provided lateral restraints for the column and limited its lateral deformation, which could improve its bearing capacity to a certain extent.

3.3. Strain Analysis

At the initial loading stage, the axial load increased linearly with increasing strain in the form of a straight line. When approaching 60–80% of the peak load, the stiffness of the material decreased, and the rise in stress was also reduced and showed a curved pattern. When the load fell to about 60–70% of the peak load, the decreasing speed of the falling section slowed down, and the specimen gradually lost its load−bearing capacity until it was destroyed.

3.3.1. Stirrup Strain

The change in the strain curve of the stirrup can reflect the restraint effect on the concrete, and the axial load–strain curves of the stirrup are shown in Figure 10.

(1) Effect of Prefabricated Shell material on load−strain curve

The influence of prefabricated shell materials on the axial load−stirrup strain curve is shown in Figure 10. It can be found that in the initial stage of test loading, for specimens ECCT−01 and RCT−01, the initial strain of both specimens maintained a linear increase, and the development laws of the curves were basically similar. The stirrup strain increased slowly in the early stage of loading. After the axial load reached 80% of the peak load, the increase rate of the stirrup strain increased greatly; the rising slope of the curve of RCT−01 was larger than that of ECCT−01, and after the peak load, the descending slope (absolute value) of the curve of RCT−01 was smaller than that of ECCT−01. As listed in Table 6, RCT−01 yielded earlier than ECCT−01. The HPFRCC-material-prefabricated shell had an effect on the axial compressive capacity of the specimen. The HPFRCC-prefabricated shell could better cooperate with the stirrups to provide more restraint and delay the yielding of the stirrups. Then, the constraint effect improved.

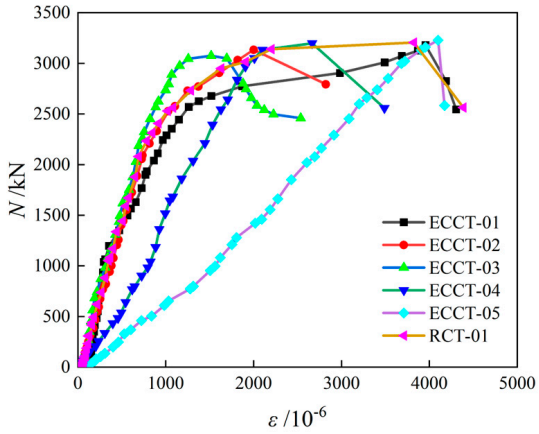


Figure 10. Stress–strain curves of stirrups.

(2) Effect of longitudinal reinforcement ratio on the load−strain curve

The influence of different longitudinal reinforcement ratios on the axial compression load−stirrup strain curve is shown in Figure 10. For specimens ECCT−01, ECCT−04, and ECCT−05, both ECCT−01 and ECCT−04 maintained a linear increase in the initial strain, and the curve development laws were basically similar. ECCT−05 maintained linear growth until peak load. The stirrup strain of ECCT−01 and ECCT−04 increased slowly in the early stage of loading. When the axial load reached 80% of the peak load, the strain increase rate of the stirrup increased significantly. The rising slopes of the curves of ECCT−01, ECCT−04, and ECCT−05 decreased successively. After the peak load, the descending slopes (absolute value) of the curves of ECCT−05, ECCT−01, and ECCT−04 decreased in turn; the stirrup of ECCT−01 yielded first, followed by that of specimen ECCT−04, and the stirrup of ECCT−05 had no apparent yield phase. The longitudinal reinforcement ratio had a significant impact on the axial compressive capacity of the specimen and the peak strain of the corresponding longitudinal reinforcement. The increase in the longitudinal reinforcement ratio could effectively delay the stirrup's yielding and improve the stirrup's restraint effect.

Table 6. Stirrup strain.

Test Piece Number	Yield Load/kN	Stirrup Strain/10^{-6}
ECCT−01	2625.35	1376.26
ECCT−02	2904.47	1607.97
ECCT−03	2568.13	886.01
ECCT−04	2670.92	1705.22
ECCT−05	2738.34	3406.50
RCT−01	2561.32	1082.85

(3) Effect of volume stirrup ratio on the load−strain curve

The influence of different volume stirrup ratios of ECCT−01, ECCT−02, and ECCT−03 on the axial load−stirrup strain curve is shown in Figure 10. Specimens ECCT−01, ECCT−02, and ECCT−03 all maintained a linear increase in the initial strain, and the overall curve development law was basically similar. The stirrup strain of the three specimens increased slowly in the early stage of loading, and when the axial load reached 80% of the peak load, the increase rate of the stirrup strain increased significantly. The rising slopes of the curves of ECCT−01, ECCT−02, and ECCT−03 increased successively. After the peak load, the descending slopes (absolute value) of the curves of ECCT−01, ECCT−03, and ECCT−02 decreased in turn. The stirrups of ECCT−03 yielded first, followed by that of specimen ECCT−0, and the stirrup of ECCT−02 yielded last. It can be seen in Figure 10 that when the stirrups of the three specimens reached yielding, specimen ECCT−02 had the highest load value.

3.3.2. Longitudinal Rebar Strain

(1) Effect of formwork material on load−strain curve

The influence of different formwork materials on the axial load−longitudinal reinforcement strain curve is shown in Figure 11. Comparing ECCT−01 and RCT−01, it can be found that in the initial stage of test loading, both initial strains maintained a linear increase, and the development laws of the curves were basically similar. The strain of the longitudinal reinforcement increased slowly in the early stage of loading, and after the axial load reached 80% of the peak load, the strain increase rate of the longitudinal reinforcement increased significantly. The rising slope of the curve of RCT−01 was larger than that of ECCT−01, and the stirrups of RCT−01 yielded earlier than that of specimen ECCT−01 and reached the peak strain faster. It can be seen in Table 7 that the material of the outer shell showed a certain influence on the axial compression bearing capacity of the specimen and had a greater influence on the peak strain of the longitudinal reinforcement. The HPFRCC material can better cooperate with the longitudinal reinforcement to delay its yielding. The performance of HPFRCC material enhanced the bearing capacity and the deformation capacity of the column members.

(2) Effect of longitudinal reinforcement ratio on load−strain curve

The influence of different longitudinal reinforcement ratios on the axial load−longitudinal strain curve is shown in Figure 11. The curve development laws of ECCT−01 and ECCT−04 were similar. The strain of longitudinal reinforcement of ECCT−05 increased slowly linearly in the early stage of loading. When the axial load reached 80% of the peak load, the strain growth rate of the longitudinal reinforcement increased significantly. In the ascending segment of the curves, the curve slope of ECC−01 was smallest, and the slope of ECC−05 was largest. As the reinforcement ratio increased, the reinforcement strain increased slower. The reinforcement ratio had a certain influence on the axial compression bearing capacity of the specimen and the peak strain of the corresponding longitudinal reinforcement. The increase in the reinforcement ratio of the longitudinal reinforcement can improve the ultimate bearing capacity of the specimen to a certain extent.

(3) Effect of volume stirrup ratio on load−strain curve

The influence of different volume stirrup ratios of ECCT−01, ECCT−02, and ECCT−03 on the axial load−longitudinal reinforcement strain curve is shown in Figure 11. Comparing ECCT−01, ECCT−02, and ECCT−03, three specimens all maintained a linear growth in the initial strain, and the overall curve development law was basically similar. The longitudinal reinforcement strains of ECCT−02 and ECCT−03 increased slowly in the early stage of loading. When the axial load reached 80% of the peak load, the strain increase rate of the stirrup was greatly increased. It can be seen that with the increase in the volume stirrup ratio, the peak load of each specimen gradually increased, and the restraint effect on the longitudinal reinforcement was greater, making the specimen yield later. And the deformation ability of the specimen was enhanced.

Table 7. Longitudinal rebar strain.

Test Piece Number	Yield Load/kN	Yield Pressure Strain/10^{-6}	Peak Load/kN	Peak Pressure Strain/10^{-6}
ECCT−01	2625.35	−5177.29	3179.82	−5949.01
RCT−01	2561.32	−1768.34	3204.43	−2214.56

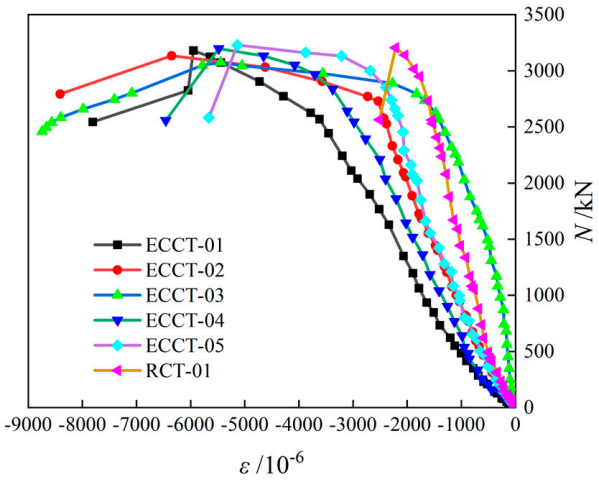


Figure 11. Stress–strain curve of longitudinal rebars.

3.3.3. Concrete Strain

The axial load−concrete/HPFRCC strain curves of the specimens are shown in Figure 12. The load−strain development curves of the specimens basically increased linearly at the initial stage of loading.

(1) Effect of Prefabricated Shell material on load−strain curve

The influence of different prefabricated shell materials on the axial load−concrete/HPFRCC strain curves is shown in Figure 12. Comparing ECCT−01 and RCT−01, both initial strains maintained a linear increase in the initial stage of test loading, and the development laws of the curves were basically similar. The curve slope of the rising section of ECCT−01 was larger than that of RCT−01. Under the same load, the HPFRCC strain of ECCT−01 was less than that of RCT−01. Thus, the concrete strain of RCT−01 at peak load was much larger than that of ECCT−01. This indicated that the HPFRCC-prefabricated shell could maintain the deformation of the column specimen better and improve the deformation performance of the composite column. Thus, failure of the composite column was postponed.

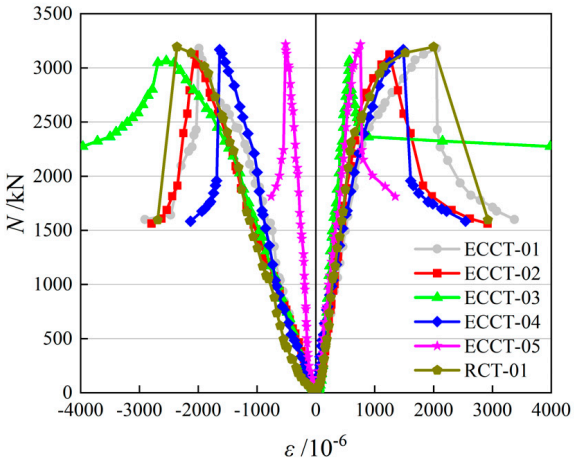


Figure 12. Load–concrete/HPFRCC strain curve.

(2) Effect of longitudinal reinforcement ratio on the load−strain curve

The influence of different longitudinal reinforcement ratios on the axial load−concrete/HPFRCC strain curves is shown in Figure 12. For ECCT−01, ECCT−04, and ECCT−05, the development laws of the curves of the three specimens were basically similar. The rising slopes of the curves of ECCT−01, ECCT−04, and ECCT−05 increased successively. Under the same load, the longitudinal reinforcement strain of the ECCT−01 was largest, while the longitudinal reinforcement strain of the ECCT−05 was smallest. The increase in the longitudinal reinforcement ratio had the effect of restricting the deformation of concrete and increasing the axial bearing capacity.

(3) Effect of volume stirrup ratio on load−strain curve

The influence of different volume stirrup ratios on the axial load−concrete strain curve is shown in Figure 12. Comparing ECCT−01, ECCT−02, and ECCT−03, the strains of the three specimens all maintained linear growth at the initial stage, and the overall curve development laws are basically similar. The HPFRCC strains corresponding to the peak load of ECCT−02, ECCT−01, and ECCT−03 increased successively. It can be seen that with the increase in the volume stirrup ratio, constraint strain capacity was improved, and there was an obvious difference in the concrete strain when ECCT−01, ECCT−02, and ECCT−03 reached the peak load.

4. Conclusions

Through axial compression tests of five HPRCC-prefabricated monolithic composite columns and one RC-prefabricated monolithic composite column, the effects of prefabricated shell material, volume stirrup ratio, and longitudinal reinforcement ratio on the mechanical properties of the composite columns were studied. The following preliminary conclusions can be drawn:

(1) The volume stirrup ratio of the HPFRCC composite column greatly influenced the deformation capacity of composite columns. As the volume stirrup ratio increased, the compressive strain corresponding to the relevant load of the composite column was greater and the deformation performance was better. Compared with ECCT−01 (ρ_v = 1.05%), the compressive strain corresponding to the yield load of ECCT−02 (ρ_v = 1.48%) increased by 24.21%, and the compressive strain corresponding to the yield load of ECCT−03 (ρ_v = 0.74%) decreased by 25.58%.

(2) As the longitudinal reinforcement ratio increased, the axial bearing capacity increased. The longitudinal reinforcement ratio had a certain influence on the axial compression bearing capacity and strain of the column specimen. Compared with ECCT−01, the peak load of ECCT−04 increased by 0.6% and the peak load of ECCT−05 increased by 1.4%.

(3) The HPFRCC-prefabricated shell composite column had a better deformation performance than the RC-prefabricated shell composite column. The HPFRCC-prefabricated shell could significantly improve the deformation properties of the composite column specimens. The compressive strain corresponding to the yield load of the HPFRCC-prefabricated shell composite column was 23.85% higher than that of the RC-prefabricated shell composite column, and the compressive strain corresponding to the peak load increased by 26.72%.

(4) The HPFRCC material shell could improve the restraint effect on the column specimen. It played a certain role in optimizing the failure mode of the composite columns. The HPFRCC-material-prefabricated mold shell could avoid brittle failure and improve the integrity of the composite column.

Using HPFRCC-material-prefabricated shells can effectively improve the deformation performance of composite columns. The volume stirrup ratio and longitudinal reinforcement ratio can significantly affect the deformation performance of HPFRCC composite columns. Due to the limited experimental conditions and data, extended parameters of the

HPFRCC-prefabricated composite column should be studied to provide a theoretical basis for its application.

Author Contributions: Conceptualization, H.J. and T.L.; methodology, K.G.; software, H.J.; writing—original draft preparation, H.J.; writing—review and editing, H.J. and T.L.; visualization, T.L.; supervision, T.L.; project administration, K.G.; funding acquisition, T.L. All authors have read and agreed to the published version of the manuscript.

Funding: This research was funded by the Natural Science Basic Research Program of Shaanxi Province, China (Grant No. 2021JQ-873); the Research Project of the Youth Innovation Team Construction of the Shaanxi Provincial Department of Education, China (Grant No. 21JP140); and the High-level Talents Fund of Xijing University, China (Grant No. XJ20B08).

Data Availability Statement: The data used to support the findings of this study are available from the corresponding author upon request.

Acknowledgments: The authors would like to acknowledge the Shaanxi Provincial Key Laboratory of Concrete Structure Safety and Durability for the equipment support and the supervisor for the guidance of the experimental process.

Conflicts of Interest: The authors declare no conflict of interest.

References

1. Zhang, B.; Hu, H.S.; Yang, Z.J.; Yang, J.Z. Axial Compressive Behavior of Ultra-High-Strength Steel Fiber-Reinforced Concrete-Filled Square Steel Tube Columns. *J. Build. Mater.* **2023**, *26*, 547–554.
2. Cui, L.S.; Jiao, C.J.; Li, S.; Tan, S.Z.; Jian, C. Experimental Investigation on Axial Compression of CFRP Confined RPC Filled Steel Tube Short Column. *J. Build. Mater.* **2020**, *23*, 852–857, 888. (In Chinese) [CrossRef]
3. Wang, J.; Chen, X.; Li, X.; Jia, Y.M. Static Experimental on Reinforced Concrete Frame Structures with Steel Fiber RPC Permanent Pillar. *J. Shenyang Jianzhu Univ. Nat. Sci. Ed.* **2014**, *30*, 9–17. (In Chinese)
4. Gao, S.L.; Xu, S.L. Experimental research on tension property of polyvinyl alcohol fiber reinforced cementitious composites. *J. Dalian Univ. Technol.* **2007**, *47*, 233–239. (In Chinese) [CrossRef]
5. Liang, X.W.; Xu, J.; Xing, P.T.; Deng, M.K. Experimental Study and Numerical Simulation on The Seismic Behavior of Fiber Reinforced Concrete Columns. *Eng. Mech.* **2016**, *33*, 66–76, 92. (In Chinese) [CrossRef]
6. Liu, Z.J.; Li, Y.; Wen, C.G. Experimental Study on Strength and Deformation Performance of PVA-ECC under Splitting Tension. *J. Build. Mater.* **2016**, *19*, 746–751. (In Chinese) [CrossRef]
7. Wang, Z.B.; Zuo, J.P.; Zhang, J.; Feng, L.L.; Jiang, G.H. Mechanical Properties of Hybrid Fiber Reinforced Engineered Cementitious Composites under Uniaxial Compression. *J. Build. Mater.* **2018**, *21*, 639–644. (In Chinese) [CrossRef]
8. Victor, C.L. High-Performance and Multifunctional Cement-Based Composite Material. *Engineering* **2019**, *5*, 250–260, 279–290.
9. Yang, P.H.; Liang, X.W.; Xin, L.; He, W. Seismic Fragility Analysis of HPFRC Energy Dissipation Wall-RC Frame Structure. *J. Build. Mater.* **2022**, *25*, 270–277. (In Chinese) [CrossRef]
10. Daugevicius, M.; Valivonis, J. Concrete and Reinforced Concrete Elements Strengthened with HPFRCC. *KSCE J. Civ. Eng.* **2018**, *22*, 2961–2969. [CrossRef]
11. Liang, X.W.; Shi, J.C.; Yu, J.; Li, L. Seismic Behavior of Reinforced Concrete Columns with Permanent Template of Ultra-High-Performance Concrete. *J. Earthq. Eng.* **2020**, *42*, 579–588, 606. (In Chinese) [CrossRef]
12. Cheng, T.; Li, N.J.; Chen, G.M.; Li, Z.B.; Xiong, Y.; Zhao, X.Y. Experimental study on axial compressive mechanical properties of concrete-filled steel tube with ECC layer reinforced by textile. *J. Xi'an Univ. Archit. Technol. Nat. Sci. Ed.* **2022**, *54*, 202–210. (In Chinese) [CrossRef]
13. Cai, J.M.; Pan, J.L.; Li, X.P. Behavior of ECC-encased CFST columns under axial compression. *Eng. Struct.* **2018**, *171*, 1–9. [CrossRef]
14. Li, F.H.; Feng, Z.H.; Deng, K.L. Axial behavior of reinforced PP-ECC column and hybrid NSC-ECC column under compression. *Eng. Struct.* **2019**, *195*, 223–230. [CrossRef]
15. Wang, X.L.; Zhao, Y.K.; Wang, L.C.; Luo, P.C.; Fan, J.J. Compressive Behavior of RC Columns Strengthened by High-Strength Steel Stranded Wire Meshes/ECC under Small Eccentric Compression. *J. Build. Mater.* **2023**, *26*, 29–36, 44. (In Chinese) [CrossRef]
16. Bert, C.W.; Malik, M. Differential quadrature: A powerful new technique for analysis of composite structures. *Compos. Struct.* **1997**, *39*, 179–189. [CrossRef]
17. Wang, Y.Y.; Gu, Y.; Liu, J.L. A domain-decomposition generalized finite difference method for stress analysis in three-dimensional composite materials. *Appl. Math. Lett.* **2020**, *104*, 106226. [CrossRef]

18. Kefal, A.; Tabrizi, I.E.; Tansan, M.; Kisa, E.; Yildiz, M. An experimental implementation of inverse finite element method for realtime shape and strain sensing of composite and sandwich structures. *Compos. Struct.* **2021**, *258*, 113431. [CrossRef]
19. Kabir, H.; Aghdam, M.M. A robust Bézier based solution for nonlinear vibration and post-buckling of random checkerboard graphene nano-platelets reinforced composite beams. *Compos. Struct.* **2019**, *212*, 184–198. [CrossRef]

Disclaimer/Publisher's Note: The statements, opinions and data contained in all publications are solely those of the individual author(s) and contributor(s) and not of MDPI and/or the editor(s). MDPI and/or the editor(s) disclaim responsibility for any injury to people or property resulting from any ideas, methods, instructions or products referred to in the content.